ACS Chemical Neuroscience

Research Article

pubs.acs.org/chemneuro

Oligo(*p*-phenylene ethynylene) Electrolytes: A Novel Molecular Scaffold for Optical Tracking of Amyloids

Patrick L. Donabedian,[†,§] Thao K. Pham,[‡] David G. Whitten,[*,‡,§] and Eva Y. Chi[*,‡,§]

[†]The Nanoscience and Microsystems Engineering Program, [‡]Department of Chemical and Biological Engineering, and [§]The Center for Biomedical Engineering, University of New Mexico, Albuquerque, New Mexico 87131, United States

Supporting Information

ABSTRACT: Finding new optical probes to detect and track amyloid protein aggregates is key to understanding and defeating the myriad of neurodegenerative and other diseases associated with these misfolded proteins. Herein we report that a series of fluorescent, soluble oligo(*p*-phenylene ethynylene)s (OPEs) are able to detect amyloids *in vitro* by massive binding-activated superluminescence, with low micromolar affinity and high selectivity for the amyloid conformer. The OPEs track the kinetics of amyloid fibril formation from native hen egg white lysozyme (HEWL) similarly to thioflavin T (ThT), and the dependence of binding affinity on OPE length supports the theory of a linear binding groove. We hypothesize, based on spectral properties, induced circular dichroism, and previous work in analogous systems, that the fluorescence turn-on mechanism is a combination of the reduction of static solvent-mediated quenching at the ethyl ester end groups of the phenylene ethynylene fluorophore and the formation of chiral J-type aggregates templated on the amyloid fibril surface.

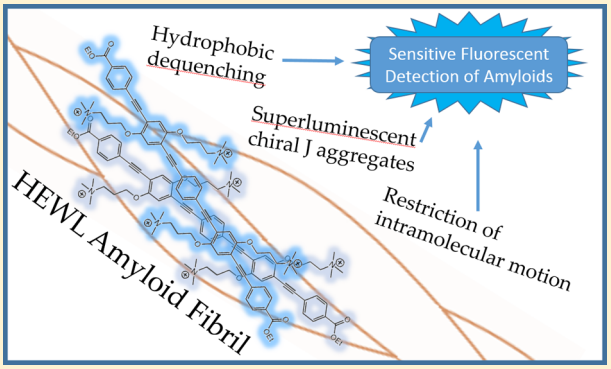

KEYWORDS: *Alzheimer's disease, amyloid diseases, protein aggregate detection, amyloid fibril staining, fluorescent optical probes, J aggregates, conjugated oligoelectrolytes*

The formation of β-sheet-rich inclusions of aggregated protein is a common feature of several diseases, notably Parkinson's disease, Huntington's disease,[1] type II diabetes,[2] the prion-transmitted spongiform encephalopathies, a variety of heritable amyloidoses, and most importantly Alzheimer's disease (AD).[3] Collectively termed the amyloidoses or proteinopathies, these diseases involve many different protein monomers with a wide variety of sizes, functions and structures, but the aggregates, "amyloids", deposited in affected organs share cross-β structure and a linear fibrous morphology with the fibril axis perpendicular to the individual β-sheet strands.[4,5] The neurodegenerative proteinopathies are especially costly to society, particularly Alzheimer's disease, which is the most common form of dementia,[6] projected to affect 13.8 million people in the United States alone by 2050.[7] The primary histopathological sign of Alzheimer's disease is the presence of extracellular plaques of amyloid-β peptide and intracellular "neurofibrillary tangles" composed of hyperphosphorylated tau protein, both of which aggregates possess amyloid character.[8,9] Parkinson's disease, another amyloid neuropathy, is associated with neuronal formation of aggregates of the α-synuclein protein and the preferential death of dopamine-producing neurons, and like Alzheimer's disease, its pathology is still contested across the literature.[10]

Regardless of the details of amyloid pathology in neurodegenerative and other diseases, monitoring the course of amyloid formation at the biochemical, cellular, and tissue levels, both in humans and in animal models, is vital to understanding and combating proteinopathies[11] and remains an unmet challenge. Though conformation- and sequence-specific antibodies have been developed for amyloid applications,[12] the primary means of detecting and localizing amyloid aggregates are small-molecule probes, whether fluorescent ligands, radiolabeled ligands for positron-emission tomography (PET)[13] and single photon emission computed tomography (SPECT), or metal-ligated magnetic resonance imaging (MRI) contrast agents.[14] Fluorescent ligands are especially attractive because of their inherently lower capital costs, their lack of radioactivity and the detailed chemical and structural information that can be extracted from the spectral properties of a bound molecule. A variety of chemical and photophysical properties may be desirable in an amyloid fluorescent biomarker.[15] First, the compound must bind to the amyloid fibril protein conformation with high affinity and specificity. Compounds that bind specifically to amyloid tend to share a common molecular profile with a "rigid conjugated rod" morphology; computational studies have shown that linear shape and aromaticity are favorable for binding to hydrophobic surface grooves in the

Received: March 12, 2015
Accepted: June 26, 2015
Published: June 26, 2015

DOI: 10.1021/acschemneuro.5b00086
ACS Chem. Neurosci. 2015, 6, 1526−1535

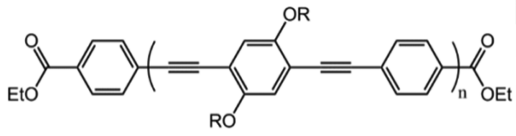

Comp.	n	R
OPE1+	1	$(CH_2)_3N(CH_3)_3^+$
OPE2+	2	$(CH_2)_3N(CH_3)_3^+$
OPE3+	3	$(CH_2)_3N(CH_3)_3^+$
OPE1-	1	$(CH_2)_3SO_3^-$

Figure 1. Structure and functional groups of OPEs used in this study.

amyloid fibril;[16] similar binding modes have been supported by scanning tunneling microscopy.[17] Past studies of amyloid-specific probes have investigated molecular scaffolds derived[18] from Congo red/curcumin,[19−21] thioflavin T,[22−24] oligothiophenes,[25−31] or other scaffolds.[32−34] These ligands, when used for fluorescent imaging, primarily function on a "molecular rotor" basis, in which fluorescence enhancement and emission red shift is accomplished by planarization of the conjugated region and prevention of rotation within the fluorophore when bound to a planar site on the amyloid fibril surface. Studies have targeted various properties, such as appropriate pharmacokinetics for *in vivo* imaging, detection of pre-thioflavinophilic amyloids, structural differentiation of amyloids with different precursors or properties, two-photon imaging, or near-infrared excitation and emission.

Oligo(*p*-phenylene ethynylene) electrolytes (OPEs), which have been previously investigated along with their polymeric derivatives for a variety[35,36] of antimicrobial[37−40] and sensing[41−44] applications as well as for organic semiconductor devices, have many of the desirable properties for amyloid biomarkers, such as linear, highly conjugated morphology and several well-characterized fluorescence sensing effects. Compared with the currently used amyloid dyes such as thioflavin T and Congo red, OPEs offer the additional advantage of being highly versatile. The chemical, structural, and material properties of OPEs can be easily tailored by synthesizing compounds with different side and end groups as well as number of repeat units. In addition to the molecular-rotor motif of optical sensing, OPEs also offer additional modes of molecular sensing giving rise to distinct fluorescence signatures. The compounds can form supramolecular aggregates of different types[43] with distinct spectral characteristics, such as J aggregates, upon binding to substrates. J, or Jelley, aggregation is a mode of dye complexation with characteristic bathochromic absorbance shifts, sharpened fluorescence bands, enhancement of fluorescence yield, and narrowed Stokes shift. These aggregates have a long history in dye chemistry, and recent reviews[46] can provide more detailed background. The exact structure of J-type aggregates varies somewhat with the dye and "brickwork", "ladder", and "staircase"-type arrangements have all been proposed.[46] OPEs with charged moieties pendant on the sides of the phenylene ethnylene (PE) backbone, rather than the ends, have been previously found to preferentially form J aggregates when complexed with oppositely charged surfactants.[45] Formation of such aggregates gives OPEs one mechanism of turn-on fluorescence sensing, which can be termed aggregation-enhanced emission.[47] In addition, ethyl ester termini have been shown to confer strong excited-state quenching of fluorescence by water: quantum yield of a cationic OPE with symmetric ethyl ester termini (OPE1+, Figure 1) increases from 2.3% in water to 5% in deuterium oxide[48] and over 75% in methanol[49] (Table 2). This effect vanishes when the ester is converted to a free carboxylate and could be due to a hydrogen bonding or partial proton transfer mechanism.[48] These various effects give OPEs several distinct ways to provide spectral information about their environment and conformation, stemming from the one degree of rotational freedom in the ethynyl−aryl bonds, several different solvent quenching effects, Coulombic interactions with the charged groups, and hydrophobic interactions with the conjugated backbone. These molecular and optical properties, and their similarity to the "rigid conjugated rod" morphology, led us to test OPEs as selective optical sensors for amyloids. In the present study, we selected four OPE molecules (Figure 1) with ethyl ester termini and varying charge and number of repeat units and successfully applied them *in vitro* as fluorescent probes specific for model amyloids formed from hen egg white lysozyme. We expect to use this study as a starting point for future investigation of phenylene ethynylene-like molecules as sensors for amyloids in a wide variety of *in vitro* and *in vivo* settings using single- and multiphoton excitation.

RESULTS AND DISCUSSION

Four OPEs (Figure 1) were chosen from our library of compounds for evaluation against HEWL amyloids. The OPEs used, designated for brevity OPE*n*+ and OPE1−, all have ethyl ester terminal moieties on the PE backbone and charged side-pendant groups; the cationic compounds have n = 1, 2, and 3 repeat units, and the anionic compound has one repeat unit. The compounds are amphiphilic and water-soluble due to the hydrophobic backbone and charged side groups. These ester-terminated compounds were selected for the effective sensing modality of fluorescence yield increase from reduced quenching by water when bound to a hydrophobic surface.

Formation and Characterization of HEWL Amyloids. Hen egg white lysozyme (HEWL) was used to form fibrillar amyloid aggregates for use in this study. Lysozyme has been suggested[50] as a useful model protein for amyloid studies, due to its low cost and the relative ease with which it can be induced to form amyloid aggregates. Lysozyme amyloid oligomers and fibrils have also been shown to exhibit cytotoxicity toward human neuroblastoma cells,[51] indicating that the amyloid-aggregate conformer of lysozyme recapitulates most of the relevant properties of known disease-associated proteins. For our experiments, HEWL (Sigma-Aldrich) was incubated at 70 °C and a concentration of 350 μM in pH 3 sodium citrate buffer (10 mM) with 100 mM NaCl.[52] Visible precipitates of aggregated lysozyme were observed to accumulate over the time of incubation, and the formation of amyloid fibrils was characterized by thioflavin T (ThT) fluorescence assay, far-UV circular dichroism (CD) spectroscopy, and atomic force microscopy (AFM) and transmission electron microscopy (TEM).

ThT-positive aggregates were detected by the second hour of incubation (Figure 2; kinetics parameters are summarized in Table 1), and the profile of ThT fluorescence enhancement over incubation time had the sigmoidal shape consistent with the nucleation-controlled aggregation mechanism that is well accepted for amyloid formation. Far-UV CD measurements (Figure 3) showed conversion of primarily α-helix structure of

DOI: 10.1021/acschemneuro.5b00086
ACS Chem. Neurosci. 2015, 6, 1526−1535

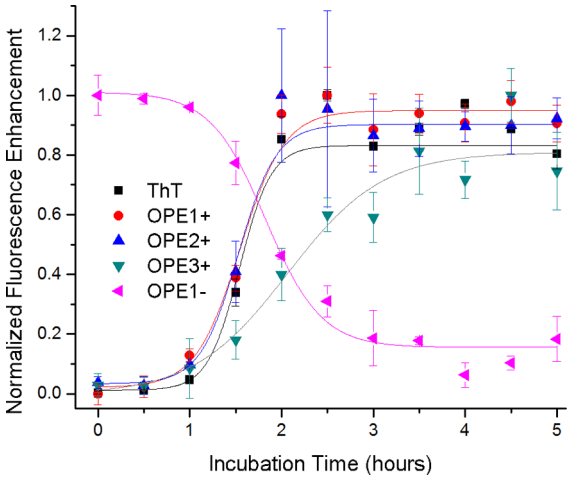

Figure 2. OPE and thioflavin T (10 μM) fluorescence enhancement profiles of HEWL incubated for various times (10 μM monomer basis, 0.5 mg/mL), with unbound dye fluorescence normalized to 0 and maximum dye fluorescence normalized to 1. Sigmoidal curves were generated by nonlinear regression to a Boltzmann sigmoid function in Origin 9. Kinetics parameters are summarized in Table 1.

Table 1. Apparent Rate Constants (k_{app}) and Lag Times (t_{lag})[a] of HEWL Fibril Formation Detected by ThT and OPEs

compound	k_{app} (h^{-1})	t_{lag} (h)
ThT	5.79 ± 2.79	1.20 ± 0.40
OPE1+	4.14 ± 0.76	1.06 ± 0.14
OPE2+	4.82 ± 0.45	1.11 ± 0.08
OPE3+	1.94 ± 0.65[b]	1.03 ± 0.52
OPE1−	3.30 ± 0.59	1.22 ± 0.16

[a]Fibril formation was monitored by ThT or OPE fluorescence. Lag times and apparent rate constants were obtained by fitting the fibril formation profiles to eq 1. [b]Difference from k_{app} of ThT value significant at $p < 0.1$.

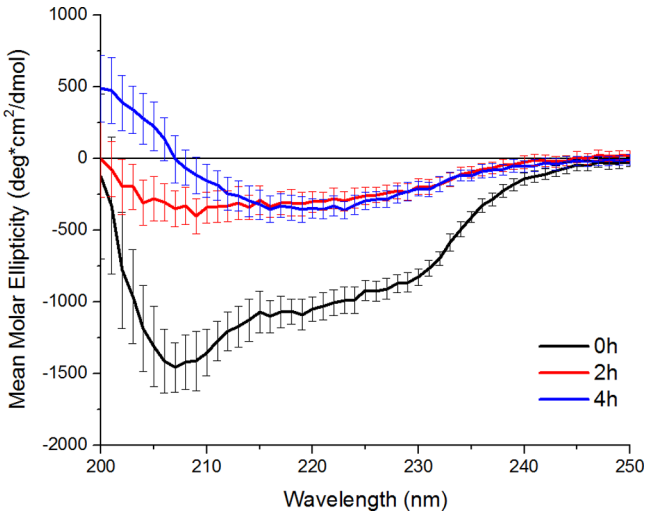

Figure 3. Far-UV circular dichroism spectra of 0, 2, and 4 h incubated HEWL (0.14 mg/mL) in pH 3 citrate buffer (10 mM).

monomeric lysozyme (0 h), as indicated by the negative bands at 222 and 208 nm, into primarily β-sheet structure in the mature aggregates (2 and 4 h), as indicated by the single negative band at 218 nm and the positive band just visible at the 200 nm edge of the spectrum.[53]

Fibrillar morphology of HEWL aggregates was visualized directly by AFM and TEM. AFM on dry mica and TEM (Figure 4) on non-glow-discharged carbon grids showed that unincubated HEWL (0 h, Figure 4a) formed a homogeneous film without large features. One hour of incubation (Figure 4b) caused the HEWL to form distinguishable bumps, hypothesized to be pre-thioflavinophilic oligomers. By 1.5 h of incubation when amyloid formation was just past the halfway point as indicated by ThT fluorescence (Figure 2), small linear aggregates were observed (Figure 4c), which lengthened by the fourth hour into short, bundled fibrils, 20−30 nm wide and 60−200 nm long (Figure 4d). No fibrils significantly longer than these were observed, even for longer incubated samples. These fibrillar, β-sheet enriched, ThT-positive HEWL amyloid aggregates were then used to evaluate the binding activity and photophysical changes of OPEs against amyloid.

Spectrophotometry of OPE−HEWL Interactions. Excitation and emission spectra of OPEs in phosphate buffer (PB) alone, with monomeric HEWL, and with HEWL amyloids (8 h incubated) are shown in Figure 5, and relevant photophysical properties are summarized in Table 2. A 10:1 molar ratio of protein to OPE was used for these experiments. Absorbance spectra were also taken (see Supporting Information, Figures S1 and S2), but background light scattering from insoluble amyloid aggregates made them difficult to interpret, so "fluorescence detected absorbance" in the form of excitation spectra was used instead. Normalized excitation and emission spectra, in which peak shifts and line shape changes of spectra are easier to visualize, are provided in the Supporting Information (Figures S3−S10). All four OPEs exhibited significant fluorescence enhancement in solution with HEWL amyloids (Figure 5e−h), and no fluorescence change with HEWL monomers except for OPE1−. The fluorescence enhancement over baseline was most significant for the longer OPE2+ and OPE3+ (Figure 5g,h), which also had notably sharpened fluorescence spectra with small (~10 nm) blue shifting of the maximum (Supporting Information, Figures S9 and S10). OPE1− had a similarly sharpened and blue shifted emission spectrum (Figure 5f and Supporting Information, Figure S8) with both HEWL monomers and amyloid, with the appearance of a shoulder at 465 nm with amyloid. OPE1+ (Figure 5e) exhibited no change in wavelength or line shape of emission spectrum, just a large increase in intensity when mixed with amyloids. The excitation spectra (Figure 5a−d) show a notable bathochromic shift for each OPE in solution mixed with amyloid, of 23, 27, 35, and 29 nm of the low-energy band for OPE1+, OPE2+, OPE3+, and OPE1−, respectively. The high-energy band, less relevant for imaging purposes, was also bathochromically shifted. Very small to no changes in excitation and emission were observed for the cationic OPEs when mixed with monomeric HEWL. The anionic OPE1− had similar excitation spectrum (Figure 5b) when mixed with monomer and amyloid, except for a moderate increase in intensity with amyloid.

A plot of normalized fluorescence enhancement for all four OPEs and thioflavin T with HEWL fibrils incubated for different lengths of time is shown in Figure 2. Following earlier examples,[54] the fibrillation kinetics was modeled as a nucleation-dependent mechanism, and data were fitted by nonlinear regression to the Bolzmann sigmoid function using Origin 9:

DOI: 10.1021/acschemneuro.5b00086
ACS Chem. Neurosci. 2015, 6, 1526−1535

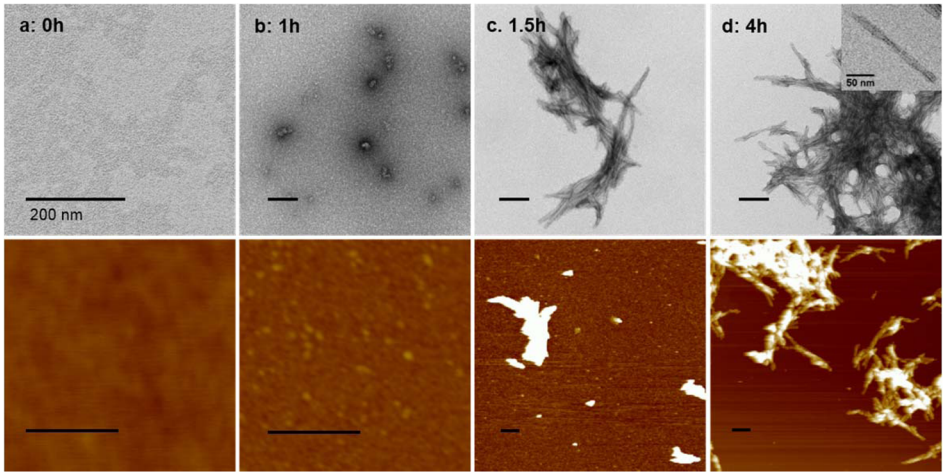

Figure 4. TEM (top) and AFM (bottom) images of 0 (a), 1 (b), 1.5 (c), and 4 h (d) incubated HEWL. Scale bars = 200 nm. Inset of panel d shows view of a single fibril, showing a twisted morphology. AFM image *Z*-height: 0 h, 25 nm; 1 h, 25 nm; 1.5 h, 15 nm; 4 h, 100 nm.

$$y = \frac{A_1 - A_2}{1 - e^{x - x_0/(dx)}} + A_2 \quad (1)$$

where y is the fluorescence intensity, x is the incubation time, x_0 is the time to 50% of maximal fluorescence, dx is the width of the fluorescence change, and A_1 and A_2 are the pre- and post-fibril formation fluorescence intensities, respectively. Thus, the apparent rate constant, k_{app}, for fibril growth is given by $1/(dx)$ and the lag time, t_{lag}, is given by $x_0 - 2dx$; values of these kinetics parameters are summarized in Table 2. As shown, all five compounds report the same lag time for HEWL amyloid formation under tested conditions, roughly 1 h. All OPEs, except OPE3+, also report fibril growth rate constants comparable to that of ThT. Interestingly, the largest compound tested, OPE3+, reports a lower rate constant ($p < 0.1$) compared with that of ThT, possibly because the binding of the compound requires larger binding sites on longer fibrils. At the equimolar concentrations used for this assay, OPE1− has greater fluorescence enhancement when mixed with monomeric species than with amyloid, giving it a profile that is the reverse of those observed for the cationic OPEs or ThT, though with the same apparent rate constant and lag time; this effect will be discussed below.

Determination of OPE/Amyloid Binding Constants. Next, binding saturation assays were conducted to quantify the affinity of OPE−amyloid binding; data and fitted curves are shown in Supporting Information Figures S11−S15, and the fitted binding constants are summarized in the last column of Table 2. Since the linear fibril binding sites could potentially fit many OPEs, binding curves were fitted to the Hill equation to capture possible binding cooperativity:

$$y = \frac{F_{max} x^n}{K^n + x^n} \quad (2)$$

where, y is OPE fluorescence intensity, x is OPE concentration (protein concentration was fixed in these assays), F_{max} is OPE fluorescence intensity at saturation, K is the equilibrium dissociation constant, and the exponential term n is the Hill parameter, which describes cooperativity of binding.[55] Fits to the data for the three cationic OPEs produced F_{max} values close to the observed fluorescence saturation values, and fitted values of K are reported in Table 2. The fits indicated that OPE1+, OPE2+, and OPE3+ bound to HEWL amyloid with low micromolar affinity moderately dependent on OPE length, with the calculated dissociation constant decreasing from 2.6 μM for OPE1+ to 1.15 μM for OPE2+, and 858 nM for OPE3+. Although the differences between binding constant for the two and three repeat unit OPEs are not statistically significant, the decrease in molar dissociation constant with increasing OPE length is consistent with the hypothesis of a linear, extended "binding groove".

Because the anionic OPE1− showed fluorescence changes with both monomeric and fibrillar HEWL, binding assays were conducted for both conformers of HEWL. In contrast to the binding curves of cationic OPEs, the binding of anionic OPE1− to HEWL monomers appeared to be linear and nonsaturable for up to 10 μM OPE concentration or a 2:1 OPE/HEWL molar ratio (Supporting Information, Figure S14), indicating a low-affinity binding to a very large number of sites. Nonspecific OPE1− binding to HEWL monomers precluded accurate determination of a binding constant for OPE1−/amyloid interactions (Supporting Information Figure S15) such that quantitative comparisons of binding between the cationic and anionic compounds cannot be made.

Induced Circular Dichroism of OPE−Amyloid Complexes. Twists are often observed in mature amyloid fibrils, including HEWL fibrils prepared in this study (Figure 4d, inset). This twist or other intrinsic chirality of the HEWL molecule might induce chirality in bound ligands. To test this hypothesis and gain further insights into the structure of bound OPE states, CD measurements were taken in the OPE absorbance range to determine whether the intrinsic chirality of the HEWL fibrils was transferred to the OPE chromophore by a chiral backbone twist or an "excitonic" chiral supramolecular aggregate. CD spectra (Figure 6) indicated that OPEs became optically active when bound to HEWL amyloids, as shown in Figure 6. As expected, no OPE had optical activity by itself in phosphate buffer solution, and nonbinding cationic OPEs were not optically active with HEWL monomers. OPE1−, which did appear to bind to monomers, though somewhat weakly, also had no optical activity. OPE1+ did not have optical activity with HEWL amyloid, but the other three OPEs did. OPE1−, OPE2+, and OPE3+ all had strong induced CD with a negative Cotton effect when bound to HEWL amyloid fibrils. OPE2+ and OPE3+ gave rise to similar CD spectra, with more intense bands in the spectrum for OPE3+.

DOI: 10.1021/acschemneuro.5b00086
ACS Chem. Neurosci. 2015, 6, 1526−1535

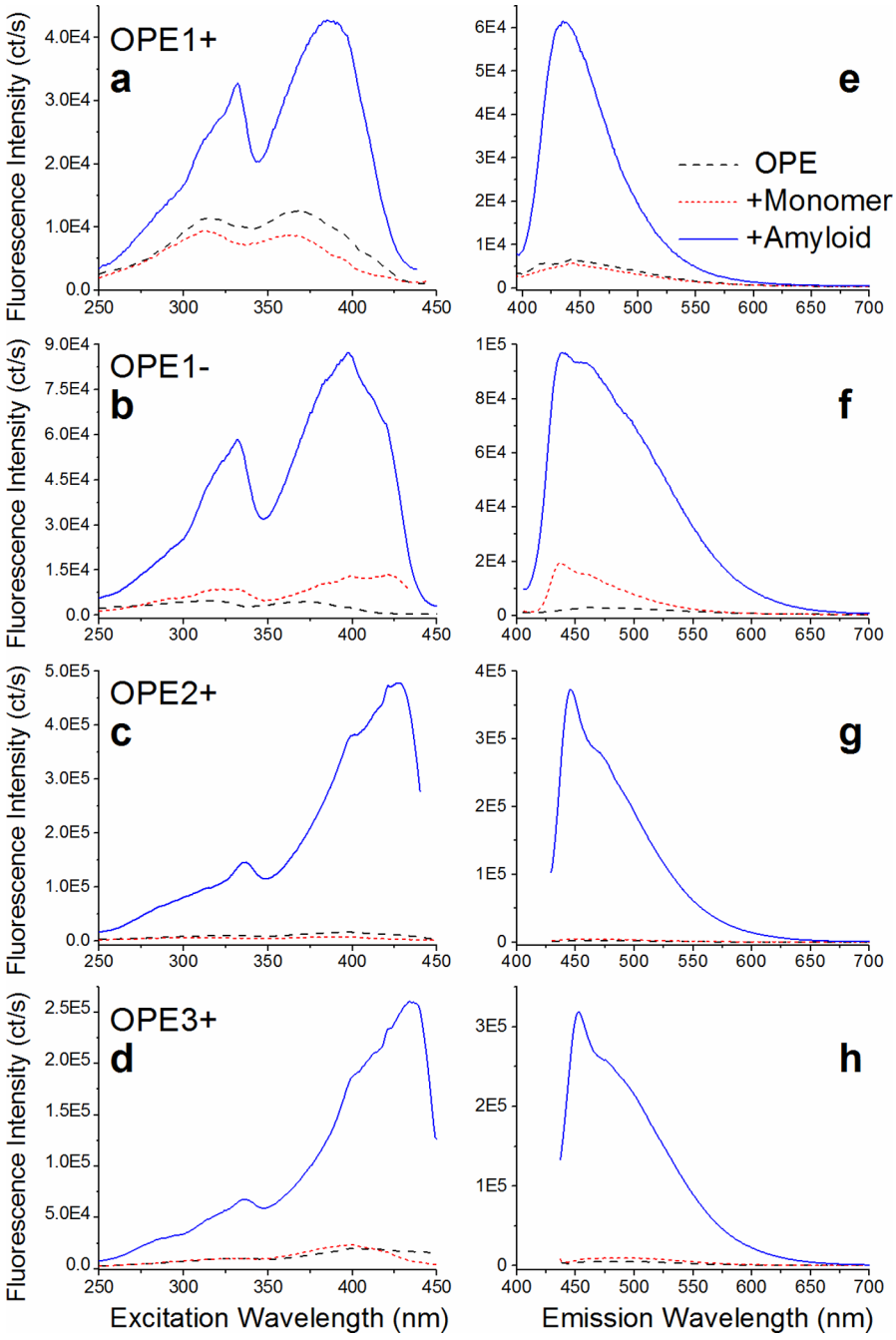

Figure 5. Excitation (a–d) and emission (e–h) spectra of OPEs (a, e, OPE1+; b, f, OPE1−; c, g, OPE2+; d, h, OPE3+) in phosphate buffer (PB, pH 7.4, 10 mM) alone (black long dashed line), with HEWL monomers (red short dashed line), and with HEWL amyloids (blue solid line). OPE concentration = 500 nM, protein concentration = 5 μM monomer basis (0.25 mg/mL). Emission and excitation wavelengths, respectively, were chosen as shown in Table 2 for each sample.

Table 2. Relevant Photophysical Properties of OPEs Alone and Bound to HEWL Amyloid, And Apparent Binding Constants (K) and Hill Coefficients (n) of OPE Binding to HEWL Amyloid

	quantum yield, φ_{fl}[a]		excitation wavelengths, λ_{ex} (nm)		emission wavelength, λ_{em} (nm)			
compd	H_2O	MeOH	PB	PB with HEWL amyloids	H_2O	PB	PB with HEWL amyloids	K (μM)
OPE1+	0.023	0.75	314, 362	332, 385	454	454	454	2.63 ± 0.58[c]
OPE2+	0.039	0.71	330, 399	337, 426	448	460	445	1.15 ± 0.26
OPE3+	0.069	0.7	340, 399	335, 434	440	464	453	0.858 ± 0.058
OPE1−			314, 370	327, 399	454	454	439[b]	

[a]From a previous study.[56] [b]Same maximum with monomer and amyloid, with the addition of a shoulder ~465 nm with amyloid. [c]Difference from other values significant at $p < 0.05$.

DOI: 10.1021/acschemneuro.5b00086
ACS Chem. Neurosci. 2015, 6, 1526−1535

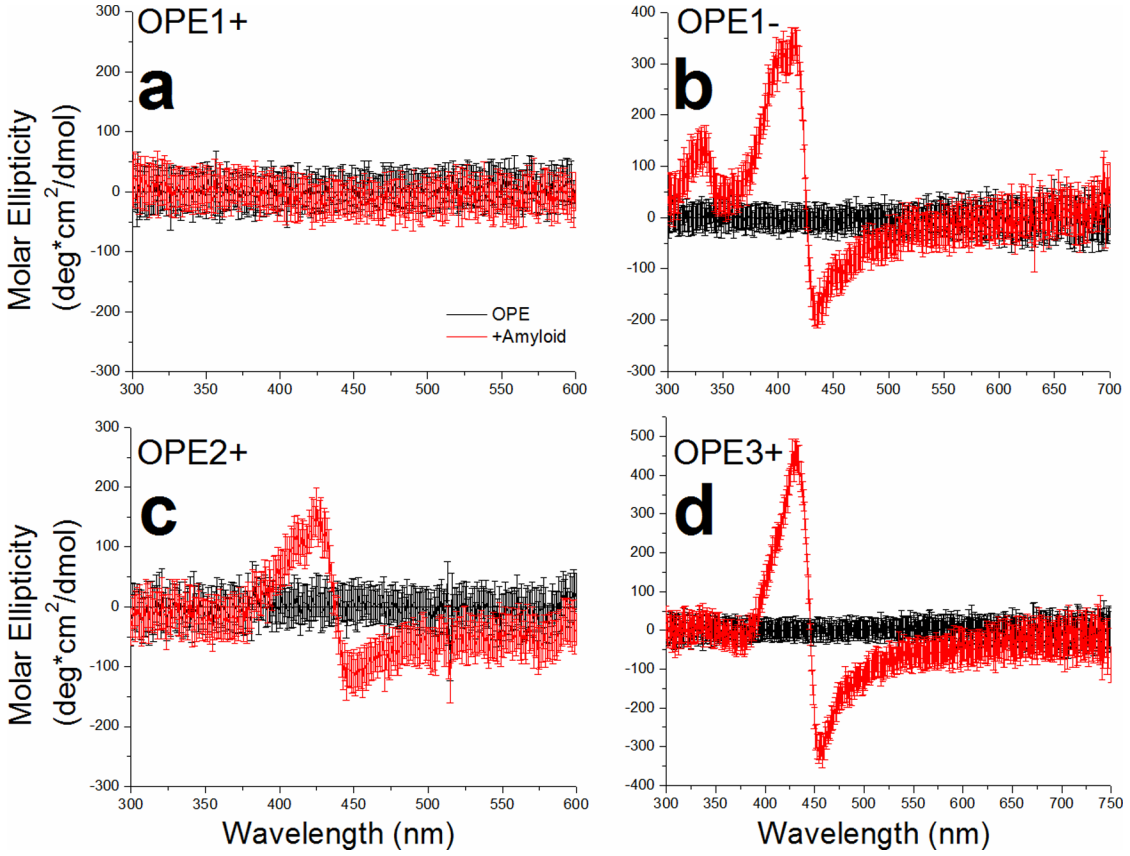

Figure 6. Circular dichroism spectra of OPEs in PB with HEWL monomer (black trace) and with HEWL amyloid (red trace): (a) OPE1+; (b) OPE1−; (c) OPE2+; (d) OPE3+. OPEs 10 μM, HEWL 10 μM on monomer basis (0.5 mg/mL).

The induced CD spectrum for OPE1− had a pronounced two-band structure, reflecting the more intense high-energy band for the anionic OPE when bound to HEWL amyloid.

Protein → OPE Energy Transfer in OPE−Amyloid Complexes. Since lysozyme is an intrinsically fluorescent protein whose emission spectrum in the 320−380 nm wavelength range overlaps significantly with the excitation spectra of OPEs (Supporting Information, Figure S21), we investigated the possibility of Förster resonance energy transfer (FRET) from the protein chromophore to OPEs by a simple spectroscopic method. Emission spectra of solutions containing OPEs and HEWL amyloids or monomers were obtained using the excitation wavelength of HEWL (280 nm), and OPE emission was observed only from OPE/amyloid samples, indicating that HEWL → OPE energy transfer was occurring only with OPEs bound to amyloid fibrils. The results are summarized as FRET efficiencies (E) in Figure 7. The raw spectral data (Supporting Information, Figures S16−S19) was converted to efficiencies by the equation:

$$E = \frac{F_A}{F_D + F_A} \tag{3}$$

where E is efficiency, F_D is the integrated area under the donor emission peak and F_A is the integrated area under the acceptor emission peak. This simple expression is valid for this case since the OPEs are nonfluorescent when excited at the donor excitation wavelength of 280 nm, eliminating crosstalk. Thus, F_A is the total number of energy transfer events, and $(F_A + F_D)$ is the total number of excitation events. Theoretically, the efficiencies should be convertible into distances by

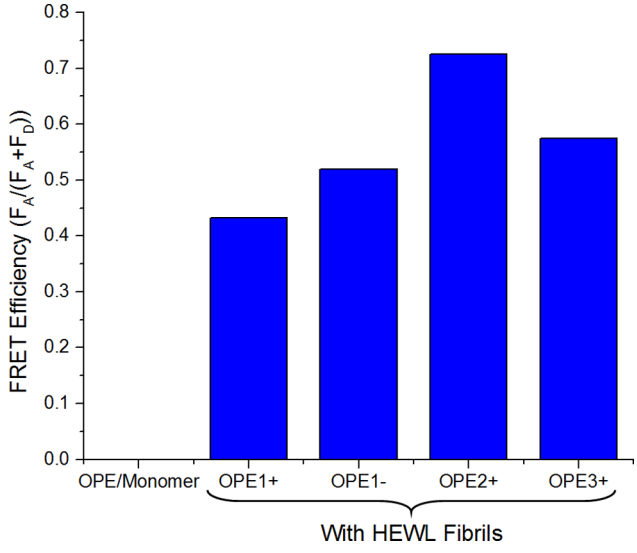

Figure 7. HEWL → OPE FRET efficiencies calculated from spectral data (Supporting Information) by eq 1. Data from control experiments can be found in Supporting Information.

$$E = \frac{1}{1 + \left(\frac{r}{R_0}\right)^6} \tag{4}$$

where r is distance and R_0 is the Förster radius. However, because OPEs and HEWL amyloids are not a well-characterized FRET pair with a defined Förster radius, R_0, and calclulating R_0 for a protein−ligand pair not freely rotating relative to each

DOI: 10.1021/acschemneuro.5b00086
ACS Chem. Neurosci. 2015, 6, 1526−1535

other in solution is rife with inaccuracies,[56] we cannot directly evaluate distances in the OPE−HEWL system. Qualitatively, some determinations could be made based on the relative measured efficiencies for the different OPEs. The measured FRET efficiency will be affected by multiple independent factors averaged over all the OPE−HEWL pairs in solution, such as the number of bound OPE molecules, the bound OPE−HEWL chromophore distance, and the spectral overlap integral, $J(\lambda)$, all of which will vary by OPE. The highest apparent efficiency observed for OPE2+ is probably the result of its higher binding constant than OPE1− or OPE1+ combined with its greater overlap integral than OPE3+.

Explicating the Mode of OPE−Amyloid Binding. The results of these experiments led us to hypothesize modes of interaction between OPEs and HEWL monomers and amyloids, as illustrated in Figure 8. All four OPEs tested were

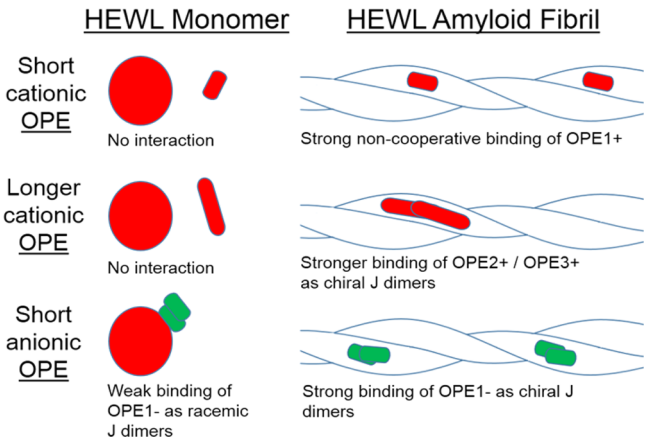

Figure 8. Illustration of proposed binding modes of OPEs to HEWL monomers and amyloid fibrils.

observed to bind to HEWL amyloid with good affinity but with different properties depending on chain length and charge. Generally, the OPEs either do not interact with protein, bind as single molecules, or bind as J dimers, which are either racemic or chirally biased. The changes in the excitation spectra of OPE2+ and OPE3+ when bound to amyloid are also highly reminiscent of the absorbance spectra observed for the same compounds when complexed with carboxymethylcellulose.[49] Overall, it has become clear that J-type aggregation is a naturally favorable mode of OPE−OPE interaction for OPEs with charged side chains when the Coulombic repulsion between the charged groups is reduced.

The spectral changes of OPE2+, OPE3+, and OPE1− in complex with HEWL amyloids and of OPE1− in complex with HEWL monomers are highly indicative of J aggregation: red-shifted absorbance, sharpening of fluorescence band, and narrowed Stokes shift. The enhancement of fluorescence intensity is attributable all or in part to the reduced quenching of the OPE by water when bound to the hydrophobic sites on the surface of the protein; this solvent-access effect is in play for all four OPEs. The current study indicates that the longer cationic OPEs, OPE2+ and OPE3+, form J dimers (or possibly larger aggregates) on the HEWL amyloid fibril surface, and OPE1− forms J dimers on both HEWL monomers and HEWL amyloid fibrils. The OPE aggregates formed on amyloid fibrils have a chiral bias to the OPE−OPE offset angle, producing a chiral supramolecular chromophore, or an excitonic optical activity, responsible for the circular dichroism seen experimentally (Figure 6). The exact source of this bias is hard to pin down; it could be a result of the helically twisted fibril axis (see Figure 4d, inset) or more specific to a binding site. Notably, the aggregates formed by OPE1− must be racemic, indicating that the OPEs are not interacting with a specific site but simply binding to oppositely charged residues on the lysozyme surface. OPE1+ exhibited some small red shifts in the excitation spectrum, but its emission spectrum does not shift at all, and it acquires no optical activity, indicating that this compound binds to HEWL fibrils as single molecules rather than as a structured aggregate. The small excitation red shift could be due to minor backbone planarization and the increase of fluorescence intensity to reduced solvent access. The results of binding saturation assays support these conclusions for the cationic OPEs. The decrease of apparent dissociation constant, K, with increasing OPE length is in agreement with the results of previous studies indicating that longer linear conjugated regions increase affinity for a long hydrophobic binding site on amyloid.[16]

One notable result of this study is the large differences between OPE1+ and OPE1− in their interactions with HEWL monomers and amyloid, as shown in Figure 8. These two single-repeat OPEs tested differ only by the charge on the side-pendant solubilizing groups (Figure 1), and their interactions with HEWL monomer and amyloids were highly different. OPE1+ exhibited noncooperative and saturable binding to amyloid fibrils without induced optical activity or large shifts in absorption or emission bands, and when bound, its emission was the least enhanced over free OPE. Its anionic counterpart, OPE1−, proved quite different both in its nonspecific binding to HEWL monomer and in its interaction with HEWL amyloid. The interaction of OPE1− with HEWL monomers has been noted in an analogous system, with sulfonate-bearing *p*-phenylene enthynylene polymers,[57] and is mediated by hydrophobic and electrostatic interactions with the positively charged (at neutral pH) lysozyme. This interaction was seen to be fairly weak and nonspecific, as indicated by the nonsaturable binding, but it overwhelms the OPE1−/amyloid interaction at high OPE concentrations, after all the amyloid binding sites are occupied. *In vitro*, without interfering effects from other cellular/tissue components, such an effect could prove useful for monitoring the disappearance of similarly charged monomers. The differences in the OPE1+ and OPE1− binding to amyloid (OPE1+ binds singly and OPE1− as chiral J aggregates) could be due to charge or H-bonding interactions specific to sites on the lysozyme fibril surface. The specificity of these possible charge effects is notable, since the arrangement of charged residues on the fibril surface is controlled by the protein's primary, secondary, and tertiary structures.

Analysis of the energy transfer from HEWL amyloids to OPEs corroborates many of these proposed binding modes. The absence of FRET in any monomer/OPE solution reconfirms the weak and nonspecific nature of OPE1−/monomer binding, since the OPE is not held within range of the fluorescing aromatic residues. In natively folded conformations of globular proteins such as lysozyme, hydrophobic residues are typically buried in the hydrophobic interior of the protein and are not solvent or ligand accessible. Aromatic residues may also only be surface exposed, available for binding, and within range of FRET to OPEs in the amyloid state; HEWL intrinsic fluorescence is found to decrease over the course of incubation (Supporting Information, Figure S22),

DOI: 10.1021/acschemneuro.5b00086
ACS Chem. Neurosci. 2015, 6, 1526−1535

which implies that the fluorescing residues are increasingly exposed to solvent quenching as more amyloid forms. The very strong distance dependence of FRET effects (typically <10 nm)[56,58] provides a strong constraint on the possible location of OPE fluorophores on the fibril surface. When combined with computational simulations, this FRET effect could shed some light on the molecular structure of other, more closely disease-related amyloid-forming proteins with intrinsic fluorescence.

CONCLUSIONS

The results of this study show that oligo(*p*-phenylene ethynylene) electrolytes are an effective molecular scaffold for selective sensing of the amyloid fibril conformer of the model protein HEWL. OPEs exhibit drastic fluorescence enhancement and useful absorbance red shift when introduced to the HEWL amyloid conformer, and binding constants were determined to be usefully low, ∼1 μM. Furthermore, the amyloid-sensing properties (fluorescence enhancement, cooperative binding, and induced optical activity) are hypothesized to be due to the propensity of the dye molecules to form chiral, super-luminescent J aggregates templated on the amyloid fibril surface. Although the OPEs used in this study were not designed or optimized for amyloid binding, they still performed as effectively as ThT, the most widely used amyloid dye. The fluorescence properties and optical activity of the bound OPEs are highly dependent on OPE chain length and charge. The longer cationic OPEs are the most promising ligands for imaging purposes among the molecules tested in this study. OPE2+ and OPE3+, in particular, have sufficiently low binding constants and optical bandgap to be used for *ex vivo* staining. On a molecular level, several effects are probably at work, including restriction of internal rotation, planarization, reduction of quenching by water, and J-type aggregation. For all four OPEs, reduction of quenching by water when bound to hydrophobic sites on HEWL is responsible for some of the drastic fluorescence enhancement. Further optimization of OPE chemical and photophysical properties may yield valuable tools for the molecular-level study of misfolded protein aggregates in a variety of diseases.

METHODS

Except OPEs, all reagents were obtained commercially and used without further purification. Synthesis of OPEs has been reported previously,[49] except for OPE1−, which was synthesized analogously to OPE1+. Hen egg white lysozyme (HEWL), thioflavin T, and buffer components were obtained from Sigma-Aldrich Chemical Co. (St. Louis, MO). All water was purified with a Synergy UV Millipore purification system (EMD Millipore, Billerica, MA). Suspensions of protein aggregates were gently vortexed to distribute aggregates before use in experiments.

Preparation of Lysozyme Amyloid Fibrils. Lyophilized HEWL was dissolved at 10 mg/mL (700 μM) in 10 mM, pH 3 sodium citrate buffer with 0.1 M NaCl. The solution was incubated in a 70 °C oil bath and magnetically stirred at 250 rpm for 12 h, and aliquots were withdrawn at half-hour intervals. The initially clear solution was observed to form cloudy aggregates by 1 h of incubation. Half of each aliquot was immediately diluted into pH 7.4 phosphate buffer to prevent further influence of acidic conditions and stored at 4 °C. The samples were observed to undergo no noticeable degradation over the course of 1 month, and these neutralized aliquots were used for all following experiments except for measurements of protein circular dichroism.

Spectrophotometry of OPE− or ThT−Protein Complexes. For studies of fluorescence enhancement vs protein incubation time, dyes were mixed with protein sample in phosphate buffer (PB, 10 mM, pH 7.4) at an equal monomer concentration of 10 μM in the wells of a standard 96-well plate. Data were fitted to the Boltzmann sigmoid function eq 1 in OriginPro 9. Emission spectra were obtained using a SpectraMax M2e plate-reading spectrophotometer (Molecular Devices, Sunnyvale, CA). Experiments were performed in duplicate, and errors are reported as standard deviation. For analysis of bound OPE excitation and emission spectra and protein−OPE energy transfer, OPEs (500 nM) were mixed with protein sample (5 μM, monomer basis) in PB, and the solution was transferred to a quartz fluorometry cuvette. Spectra were obtained on a PTI QuantaMaster 40 steady state spectrofluorometer (HORIBA Scientific, Edison, NJ).

Circular Dichroism Spectroscopy. For protein intrinsic circular dichroism, protein samples were diluted in sodium citrate buffer without NaCl (pH 3, 10 mM) to a concentration of 0.14 mg/mL, gently vortexed, and read in a 1 mm path length quartz CD cuvette using an Aviv 410 CD spectrometer (Aviv Biomedical, Lakewood, NJ) with a 15 s averaging time. A blank spectrum (PB only) was subtracted from each sample to remove background signal. Error bars are standard deviation over multiple reads of a single sample as reported by the instrument.

For OPE induced circular dichroism, OPEs and protein were diluted in phosphate buffer (pH 7.4, 10 mM) to an OPE and protein concentration of 5 μM, and data was obtained and processed identically to the protein CD experiments.

Determination of Binding Constant. For determination of binding constant of OPEs to amyloid aggregates, OPEs were mixed with HEWL amyloid in PB at a final OPE concentration ranging from 100 nM to 5 μM and final protein concentration of 5 μM (monomer basis). The solutions were then transferred to a quartz fluorometry cuvette, and emission was measured at the pertinent wavelength. Experiments were performed in duplicate, and errors were reported as standard deviation. Hill function fits to OPE binding curves were calculated using OriginPro 9.

AFM Imaging. For AFM, a droplet of each protein sample at 5 mg/mL was pipetted onto a freshly cleaved mica substrate and allowed to physisorb for 20 min, followed by a single rinse with HPLC-grade water and gentle drying under a stream of N_2. Imaging was performed with a Nanoscope IIIa AFM (Veeco, Plainview, NY) in tapping mode under a constant stream of dry N_2 gas using a rectangular silicon cantilever with a spring constant of 40 N/m (Veeco model RTESPA-W). Veeco Nanoscope software was used to capture and analyze the images. Images for 0 and 1 h are cropped from 1 μm width images subjected to a first-order *x,y* plane fit and flattened. The image at 1.5 h is cropped from a 5 μm width image subjected to a third-order *x,y* plane fit and flattened. The image at 4 h is cropped from a 5 μm width image subjected to a first-order *x,y* plane fit.

TEM Imaging. For TEM imaging, incubated HEWL solutions at a concentration of 350 μM were diluted 1:5 in water and aliquoted onto carbon-coated grids, allowed to adsorb, washed with deionized water, and stained with 2% uranyl acetate solution. Excess liquid was removed, and the samples were allowed to dry in air. Samples were imaged on a Hitatchi H7500 transmission electron microscope (Hitachi High Technologies Corp., Tokyo, Japan) with tungsten filament illumination, operating with an AMT X60 bottom mount CCD camera detector.

ASSOCIATED CONTENT

Supporting Information

Absorbance, excitation, and emission spectra of bound and unbound OPEs, saturation binding data, and spectra used to generate FRET efficiency plots. The Supporting Information is available free of charge on the ACS Publications website at DOI: 10.1021/acschemneuro.5b00086.

AUTHOR INFORMATION

Corresponding Authors

*For E.Y.C., e-mail: evachi@unm.edu.
*For D.G.W., e-mail: whitten@unm.edu.

DOI: 10.1021/acschemneuro.5b00086
ACS Chem. Neurosci. 2015, 6, 1526−1535

Author Contributions

Each author contributed equally to the research.

Funding

We gratefully acknowledge funding support from the National Science Foundation, Awards 1207362 and 1150855, Defense Threat Reduction Agency, Grant HDTRA1-08-1-0053, private giving from the Huning family of New Mexico, and Department of Education GAANN fellowship (P.L.D.).

Notes

The authors declare no competing financial interest.

■ ACKNOWLEDGMENTS

We are especially thankful to Dr. Stephen Jett of the UNM Electron Microscopy Facility for TEM imaging and to Suhyun Yoon, Lance Edens, and Dr. David Keller of UNM's Department of Chemistry and Chemical Biology for AFM imaging. Dr. Ying Wang and Dr. Arjun Thapa performed vital preliminary experimental work, and Dr. Yanli Tang and Dr. Eunkyung Ji synthesized the OPEs.

■ REFERENCES

(1) Schapira, A. H. V, Olanow, C. W., Greenamyre, J. T., and Bezard, E. (2014) Slowing of neurodegeneration in Parkinson's disease and Huntington's disease: future therapeutic perspectives. *Lancet 384*, 545−555.

(2) Westermark, P., Andersson, A., and Westermark, G. T. (2011) Islet amyloid polypeptide, islet amyloid, and diabetes mellitus. *Physiol. Rev. 91*, 795−826.

(3) Rambaran, R. N., and Serpell, L. C. (2008) Amyloid fibrils: abnormal protein assembly. *Prion 2*, 112−7.

(4) Raleigh, D. P. (2014) Guilt by Association: The Physical Chemistry and Biology of Protein Aggregation. *J. Phys. Chem. Lett. 5*, 2012−2014.

(5) Knowles, T. P. J., Vendruscolo, M., and Dobson, C. M. (2014) The amyloid state and its association with protein misfolding diseases. *Nat. Rev. Mol. Cell Biol. 15*, 384−96.

(6) Greig, N., and Lahiri, D. (2014) Editorial: Advances in Understanding Alzheimer's Disease, and the Contributions of Current Alzheimer Research: Ten Years on and Beyond. *Curr. Alzheimer Res. 11*, 107−109.

(7) Hebert, L., Weuve, J., Scherr, P., and Evans, D. (2013) Alzheimer disease in the United States (2010−2050) estimated using the 2010 census. *Neurology 80*, 1778−83.

(8) Ittner, L. M., and Götz, J. (2011) Amyloid-β and tau–a toxic pas de deux in Alzheimer's disease. *Nat. Rev. Neurosci. 12*, 65−72.

(9) Cárdenas-Aguayo, M. D. C., Gomez-Virgilio, L., DeRosa, S., and Meraz-Rios, M. A. (2014) The role of tau oligomers in the onset of Alzheimer's disease neuropathology. *ACS Chem. Neurosci. 5*, 1178−1191.

(10) Lotharius, J., and Brundin, P. (2002) Pathogenesis of Parkinson's disease: dopamine, vesicles and alpha-synuclein. *Nat. Rev. Neurosci. 3*, 932−42.

(11) Johnson, K. a, Fox, N. C., Sperling, R. a, and Klunk, W. E. (2012) Brain imaging in Alzheimer disease. *Cold Spring Harbor Perspect. Med. 2*, a006213.

(12) De Genst, E., Messer, A., and Dobson, C. M. (2014) Antibodies and protein misfolding: From structural research tools to therapeutic strategies. *Biochim. Biophys. Acta, Proteins Proteomics 1844*, 1907−1919.

(13) Jack, C. R., Barrio, J. R., and Kepe, V. (2013) Cerebral amyloid PET imaging in Alzheimer's disease. *Acta Neuropathol. 126*, 643−57.

(14) Amiri, H., Saeidi, K., Borhani, P., Manafirad, A., Ghavami, M., and Zerbi, V. (2013) Alzheimer's disease: pathophysiology and applications of magnetic nanoparticles as MRI theranostic agents. *ACS Chem. Neurosci. 4*, 1417−29.

(15) Nesterov, E. E., Skoch, J., Hyman, B. T., Klunk, W. E., Bacskai, B. J., and Swager, T. M. (2005) In vivo optical imaging of amyloid aggregates in brain: design of fluorescent markers. *Angew. Chem., Int. Ed. 44*, 5452−6.

(16) Skeby, K. K., Sørensen, J., and Schiøtt, B. (2013) Identification of a Common Binding Mode for Imaging Agents to Amyloid Fibrils from Molecular Dynamics Simulations. *J. Am. Chem. Soc. 135*, 15114−15128.

(17) Mao, X., Guo, Y., Wang, C., Zhang, M., Ma, X., Liu, L., Niu, L., Zeng, Q., Yang, Y., and Wang, C. (2011) Binding modes of thioflavin T molecules to prion peptide assemblies identified by using scanning tunneling microscopy. *ACS Chem. Neurosci. 2*, 281−287.

(18) Nilsson, K. P. R. (2009) Small organic probes as amyloid specific ligands–past and recent molecular scaffolds. *FEBS Lett. 583*, 2593−9.

(19) Zhang, X., Tian, Y., Yuan, P., Li, Y., Yaseen, M. a, Grutzendler, J., Moore, A., and Ran, C. (2014) A bifunctional curcumin analogue for two-photon imaging and inhibiting crosslinking of amyloid beta in Alzheimer's disease. *Chem. Commun. (Cambridge, U. K.) 50*, 11550−3.

(20) Zhang, X., Tian, Y., Li, Z., Tian, X., Sun, H., Liu, H., Moore, A., and Ran, C. (2013) Design and synthesis of curcumin analogues for in vivo fluorescence imaging and inhibiting copper-induced cross-linking of amyloid beta species in Alzheimer's disease. *J. Am. Chem. Soc. 135*, 16397−409.

(21) Cui, M., Ono, M., Kimura, H., Liu, B., and Saji, H. (2011) Synthesis and structure-affinity relationships of novel dibenzylideneacetone derivatives as probes for β-amyloid plaques. *J. Med. Chem. 54*, 2225−40.

(22) Ono, M., Kawashima, H., Nonaka, A., Kawai, T., Haratake, M., Mori, H., Kung, M. P., Kung, H. F., Saji, H., and Nakayama, M. (2006) Novel benzofuran derivatives for PET imaging of β-amyloid plaques in Alzheimer's disease brains. *J. Med. Chem. 49*, 2725−2730.

(23) Harrison, S. T., Mulhearn, J., Wolkenberg, S. E., Miller, P. J., O'Malley, S. S., Zeng, Z., Williams, D. L., Hostetler, E. D., Sanabria-Bohórquez, S., Gammage, L., Fan, H., Sur, C., Culberson, J. C., Hargreaves, R. J., Cook, J. J., Hartman, G. D., and Barrow, J. C. (2011) Synthesis and Evaluation of 5-Fluoro-2-aryloxazolo[5,4-b]pyridines as β-Amyloid PET Ligands and Identification of MK-3328. *ACS Med. Chem. Lett. 2*, 498−502.

(24) Yoshimura, M., Ono, M., Matsumura, K., Watanabe, H., Kimura, H., Cui, M., Nakamoto, Y., Togashi, K., Okamoto, Y., Ihara, M., Takahashi, R., and Saji, H. (2013) Structure-Activity Relationships and in Vivo Evaluation of Quinoxaline Derivatives for PET Imaging of β-Amyloid Plaques. *ACS Med. Chem. Lett. 4*, 596−600.

(25) Herland, A., Nilsson, K. P. R., Olsson, J. D. M., Hammarström, P., Konradsson, P., and Inganäs, O. (2005) Synthesis of a regioregular zwitterionic conjugated oligoelectrolyte, usable as an optical probe for detection of amyloid fibril formation at acidic pH. *J. Am. Chem. Soc. 127*, 2317−23.

(26) Arja, K., Sjölander, D., Åslund, A., Prokop, S., Heppner, F. L., Konradsson, P., Lindgren, M., Hammarström, P., Åslund, K. O. A., and Nilsson, K. P. R. (2013) Enhanced fluorescent assignment of protein aggregates by an oligothiophene-porphyrin-based amyloid ligand. *Macromol. Rapid Commun. 34*, 723−30.

(27) Klingstedt, T., Shirani, H., Åslund, K. O. A., Cairns, N. J., Sigurdson, C. J., Goedert, M., and Nilsson, K. P. R. (2013) The structural basis for optimal performance of oligothiophene-based fluorescent amyloid ligands: Conformational flexibility is essential for spectral assignment of a diversity of protein aggregates. *Chem. - Eur. J. 19*, 10179−10192.

(28) Ries, J., Udayar, V., Soragni, A., Hornemann, S., Nilsson, K. P. R., Riek, R., Hock, C., Ewers, H., Aguzzi, A. a, and Rajendran, L. (2013) Superresolution imaging of amyloid fibrils with binding-activated probes. *ACS Chem. Neurosci. 4*, 1057−61.

(29) Klingstedt, T., Aslund, A., Simon, R. a, Johansson, L. B. G., Mason, J. J., Nyström, S., Hammarström, P., and Nilsson, K. P. R. (2011) Synthesis of a library of oligothiophenes and their utilization as fluorescent ligands for spectral assignment of protein aggregates. *Org. Biomol. Chem. 9*, 8356−70.

(30) Nilsson, K. P. R., Ikenberg, K., Aslund, A., Fransson, S., Konradsson, P., Röcken, C., Moch, H., and Aguzzi, A. (2010)

DOI: 10.1021/acschemneuro.5b00086
ACS Chem. Neurosci. 2015, 6, 1526−1535

Structural typing of systemic amyloidoses by luminescent-conjugated polymer spectroscopy. *Am. J. Pathol. 176*, 563−74.
(31) Aslund, A., Sigurdson, C. J., Klingstedt, T., Grathwohl, S., Bolmont, T., Dickstein, D. L., Glimsdal, E., Prokop, S., Lindgren, M., Konradsson, P., Holtzman, D. M., Hof, P. R., Heppner, F. L., Gandy, S., Jucker, M., Aguzzi, A., Hammarström, P., and Nilsson, K. P. R. (2009) Novel pentameric thiophene derivatives for in vitro and in vivo optical imaging of a plethora of protein aggregates in cerebral amyloidoses. *ACS Chem. Biol. 4*, 673−84.
(32) Ono, M., Watanabe, H., Kimura, H., and Saji, H. (2012) BODIPY-based molecular probe for imaging of cerebral β-amyloid plaques. *ACS Chem. Neurosci. 3*, 319−24.
(33) Chang, W. M., Dakanali, M., Capule, C. C., Sigurdson, C. J., Yang, J., and Theodorakis, E. A. (2011) ANCA: A Family of Fluorescent Probes that Bind and Stain Amyloid Plaques in Human Tissue. *ACS Chem. Neurosci. 2*, 249−255.
(34) Cui, M., Ono, M., Watanabe, H., Kimura, H., Liu, B., and Saji, H. (2014) Smart near-infrared fluorescence probes with donor-acceptor structure for in vivo detection of β-amyloid deposits. *J. Am. Chem. Soc. 136*, 3388−94.
(35) Wang, Y., Schanze, K. S., Chi, E. Y., and Whitten, D. G. (2013) When worlds collide: interactions at the interface between biological systems and synthetic cationic conjugated polyelectrolytes and oligomers. *Langmuir 29*, 10635−47.
(36) Liu, Y., Ogawa, K., and Schanze, K. S. (2009) Conjugated polyelectrolytes as fluorescent sensors. *J. Photochem. Photobiol., C 10*, 173−190.
(37) Wang, Y., Canady, T. D., Zhou, Z., Tang, Y., Price, D. N., Bear, D. G., Chi, E. Y., Schanze, K. S., and Whitten, D. G. (2011) Cationic phenylene ethynylene polymers and oligomers exhibit efficient antiviral activity. *ACS Appl. Mater. Interfaces 3*, 2209−14.
(38) Wang, Y., Jett, S. D., Crum, J., Schanze, K. S., Chi, E. Y., and Whitten, D. G. (2013) Understanding the dark and light-enhanced bactericidal action of cationic conjugated polyelectrolytes and oligomers. *Langmuir 29*, 781−92.
(39) Hill, E. H., Pappas, H. C., and Whitten, D. G. (2014) Activating the antimicrobial activity of an anionic singlet-oxygen sensitizer through surfactant complexation. *Langmuir 30*, 5052−6.
(40) Corbitt, T. S., Sommer, J. R., Chemburu, S., Ogawa, K., Ista, L. K., Lopez, G. P., Whitten, D. G., and Schanze, K. S. (2009) Conjugated polyelectrolyte capsules: light-activated antimicrobial micro "Roach Motels. *ACS Appl. Mater. Interfaces 1*, 48−52.
(41) Pinto, M. R., and Schanze, K. S. (2004) Amplified fluorescence sensing of protease activity with conjugated polyelectrolytes. *Proc. Natl. Acad. Sci. U. S. A. 101*, 7505−10.
(42) An, L., Liu, L., and Wang, S. (2009) Label-free, homogeneous, and fluorescence "turn-on" detection of protease using conjugated polyelectrolytes. *Biomacromolecules 10*, 454−7.
(43) Kushon, S., Ley, K., Bradford, K., et al. (2002) Detection of DNA hybridization via fluorescent polymer superquenching. *Langmuir 18*, 7245−7249.
(44) Liu, Y., Ogawa, K., and Schanze, K. S. (2008) Conjugated polyelectrolyte based real-time fluorescence assay for phospholipase C. *Anal. Chem. 80*, 150−8.
(45) Hill, E. H., Sanchez, D., Evans, D. G., and Whitten, D. G. (2013) Structural basis for aggregation mode of oligo-p-phenylene ethynylenes with ionic surfactants. *Langmuir 29*, 15732−7.
(46) Würthner, F., Kaiser, T. E., and Saha-Möller, C. R. (2011) J-aggregates: from serendipitous discovery to supramolecular engineering of functional dye materials. *Angew. Chem., Int. Ed. 50*, 3376−410.
(47) Hong, Y., Lam, J. W. Y., and Tang, B. Z. (2011) Aggregation-induced emission. *Chem. Soc. Rev. 40*, 5361.
(48) Hill, E. H., Evans, D. G., and Whitten, D. G. (2014) The influence of structured interfacial water on the photoluminescence of carboxyester-terminated oligo-p-phenylene ethynylenes. *J. Phys. Org. Chem. 27*, 252−257.
(49) Tang, Y., Hill, E. H., Zhou, Z., Evans, D. G., Schanze, K. S., and Whitten, D. G. (2011) Synthesis, self-assembly, and photophysical properties of cationic oligo(p-phenyleneethynylene)s. *Langmuir 27*, 4945−55.
(50) Swaminathan, R., Ravi, V. K., Kumar, S., Kumar, M. V. S., and Chandra, N. (2011) Lysozyme: A model protein for amyloid research. *Adv. Protein Chem. Struct. Biol. 84*, 63−111.
(51) Gharibyan, A. L., Zamotin, V., Yanamandra, K., Moskaleva, O. S., Margulis, B. a, Kostanyan, I. a, and Morozova-Roche, L. a. (2007) Lysozyme amyloid oligomers and fibrils induce cellular death via different apoptotic/necrotic pathways. *J. Mol. Biol. 365*, 1337−49.
(52) Mulaj, M., Foley, J., and Muschol, M. (2014) Amyloid oligomers and protofibrils, but not filaments, self-replicate from native lysozyme. *J. Am. Chem. Soc. 136*, 8947−56.
(53) Greenfield, N. (2007) Using circular dichroism spectra to estimate protein secondary structure. *Nat. Protoc. 1*, 2876−2890.
(54) Nielsen, L., Khurana, R., Coats, A., Frokjaer, S., Brange, J., Vyas, S., Uversky, V. N., and Fink, A. L. (2001) Effect of environmental factors on the kinetics of insulin fibril formation: Elucidation of the molecular mechanism. *Biochemistry 40*, 6036−6046.
(55) Goutelle, S., Maurin, M., Rougier, F., Barbaut, X., Bourguignon, L., Ducher, M., and Maire, P. (2008) The Hill equation: A review of its capabilities in pharmacological modelling. *Fundam. Clin. Pharmacol. 22*, 633−648.
(56) Sahoo, H. (2011) F??rster resonance energy transfer - A spectroscopic nanoruler: Principle and applications. *J. Photochem. Photobiol., C 12*, 20−30.
(57) Kim, I., Dunkhorst, A., and Bunz, U. H. F. (2005) Nonspecific interactions of a carboxylate-substituted PPE with proteins. A cautionary tale for biosensor applications. *Langmuir 21*, 7985−9.
(58) Piston, D. W., and Kremers, G.-J. (2007) Fluorescent protein FRET: the good, the bad and the ugly. *Trends Biochem. Sci. 32*, 407−414.

DOI: 10.1021/acschemneuro.5b00086
ACS Chem. Neurosci. 2015, 6, 1526−1535